

# Contact-induced crystallinity for high-performance soluble acene-based transistors and circuits

D. J. GUNDLACH<sup>1\*</sup>, J. E. ROYER<sup>1</sup>, S. K. PARK<sup>2</sup>, S. SUBRAMANIAN<sup>3</sup>, O. D. JURCHESCU<sup>1,2</sup>,  
B. H. HAMADANI<sup>1</sup>, A. J. MOAD<sup>4</sup>, R. J. KLINE<sup>5</sup>, L. C. TEAGUE<sup>4</sup>, O. KIRILLOV<sup>1</sup>, C. A. RICHTER<sup>1</sup>,  
J. G. KUSHMERICK<sup>4</sup>, L. J. RICHTER<sup>4</sup>, S. R. PARKIN<sup>3</sup>, T. N. JACKSON<sup>2</sup> AND J. E. ANTHONY<sup>3</sup>

<sup>1</sup>Semiconductor Electronics Division, Electronics and Electrical Engineering Laboratory, National Institute of Standards and Technology, Gaithersburg, Maryland 20899-8120, USA

<sup>2</sup>Department of Electrical Engineering, The Pennsylvania State University, University Park, Pennsylvania 16802, USA

<sup>3</sup>Department of Chemistry, University of Kentucky, Lexington, Kentucky 40506-0055, USA

<sup>4</sup>Surface and Microanalysis Science Division, Chemical Science and Technology Laboratory, National Institute of Standards and Technology, Gaithersburg, Maryland 20899-8372, USA

<sup>5</sup>Polymers Division, Material Science and Engineering Laboratory, National Institute of Standards and Technology, Gaithersburg, Maryland 20899-8541, USA

\*e-mail: david.gundlach@nist.gov

Published online: 17 February 2008; doi:10.1038/nmat2122

The use of organic materials presents a tremendous opportunity to significantly impact the functionality and pervasiveness of large-area electronics. Commercialization of this technology requires reduction in manufacturing costs by exploiting inexpensive low-temperature deposition and patterning techniques, which typically lead to lower device performance. We report a low-cost approach to control the microstructure of solution-cast acene-based organic thin films through modification of interfacial chemistry. Chemically and selectively tailoring the source/drain contact interface is a novel route to initiating the crystallization of soluble organic semiconductors, leading to the growth on opposing contacts of crystalline films that extend into the transistor channel. This selective crystallization enables us to fabricate high-performance organic thin-film transistors and circuits, and to deterministically study the influence of the microstructure on the device characteristics. By connecting device fabrication to molecular design, we demonstrate that rapid film processing under ambient room conditions and high performance are not mutually exclusive.

During the past decade, research on organic thin-film transistors (OTFTs) and related materials has resulted in significant improvements to the electrical characteristics of discrete devices and the use of OTFTs in several demonstrations of anticipated entry market applications<sup>1–7</sup>. Recent reports of high-performance solution-processed polymer TFTs (ref. 8) and ultralow-power-consumption complementary logic circuits fabricated from vapour-deposited small-molecule organic semiconductors<sup>9</sup> underscore the rapid progress in materials design and device engineering/processing. However, the former example uses a relatively high-temperature anneal step to improve molecular order for high mobility, and the latter example uses shadow masks to pattern the different organic semiconductor films and source/drain contacts. The lack of high-volume, cheap processing methods for fabricating high-performance OTFTs limits the potential for organic electronics to significantly impact the large-area electronics market<sup>10–12</sup>.

Several innovative schemes have been presented to address manufacturing challenges in depositing and patterning the materials/layers comprising an OTFT. These include the use of organic etch masks and plasma etching to define deposited layers<sup>13–15</sup>, transfer printing of materials with predefined features<sup>16,17</sup> and local deposition by direct dry printing<sup>18</sup>.

Attempts to self-pattern high-performance regions in the organic semiconductor layer have focused on modifying the gate dielectric surface using molecules that form self-assembled molecular layers and promote differential adsorption or wetting between the channel region of the device and the field regions<sup>19–22</sup>. Here, we report on high-performance OTFTs and OTFT circuits fabricated with a soluble acene derivative by using spin-coating, a rapid film-forming technique. OTFTs fabricated from films of soluble acene derivatives cast using slow film-forming techniques were demonstrated to have high field-effect mobility (exceeding  $1 \text{ cm}^2 \text{ V}^{-1} \text{ s}^{-1}$ ), making this class of materials technologically relevant for low-cost large-area flexible electronic applications<sup>23–25</sup>. We exploit the strong tendency of this class of material towards forming molecular crystals<sup>26,27</sup> to greatly improve the transistor channel mobility. By chemically tailoring the surface properties of the source/drain contacts, we are able to induce crystalline growth on the contacts that extends tens of micrometres into the transistor channel and significantly impacts the electrical characteristics of the OTFTs. Importantly, our use of the contacts to induce improved thin-film microstructure demonstrates a novel low-cost room-temperature process for self-patterning high-mobility regions in the channel of OTFTs with technologically viable dimensions. Our results are fundamentally different from the previous work

on contacts treated with self-assembled molecular layers where improvements in electronic structure or microstructure are limited to the nanometre to submicrometre length scale<sup>23,24,28–30</sup>. In addition, the unique microstructure we obtain in our films enables us to fabricate test structures that are ideal for studies correlating charge transport with thin-film microstructure.

The processing conditions used to obtain improved microstructure and OTFT electrical performance are documented in the Methods section. Figure 1a,b shows the chemical structure of fluorinated 5,11-bis(triethylsilylethynyl) anthradithiophene (diF-TESADT) and pentafluorobenzene thiol (PFBT) (ref. 23), which are the organic semiconductor and contact treatment material, respectively. Although not shown explicitly in Fig. 1a, the diF-TESADT is synthesized as an inseparable mixture (typically 1:1) of syn- and anti-isomers. The schematic cross-section of the OTFT device structure used in this study is shown in Fig. 1c.

Figure 2a shows typical drain current versus drain-to-source voltage ( $I_D$  versus  $V_{DS}$ ) characteristics for a diF-TESADT TFT with PFBT-treated contacts. The device has a channel length ( $L$ ) of 20  $\mu\text{m}$  and a channel width ( $W$ ) of 1,000  $\mu\text{m}$ . The curvature and compression of  $I_D$  at low  $V_{DS}$  (linear region of device operation) is generally attributed to contact effects<sup>28,31</sup>. Such non-ideal behaviour is commonly observed in high-mobility OTFTs because the large channel current density ( $10^4$ – $10^5$   $\text{A cm}^{-2}$ ) places great demand on the injection efficiency of the source contact. Figure 2b shows the drain current versus gate-to-source voltage ( $I_D$  versus  $V_{GS}$ ) characteristics for the same device biased in the saturation region of operation ( $V_{DS} = -60$  V). The data are plotted as  $\sqrt{I_D}$  versus  $V_{GS}$ , and the fitting line used for mobility extraction is shown (equation (1), Methods section). The straight line fits the data over a large range of  $V_{GS}$ , indicating that the OTFT is a reasonably well-behaved square-law device, although the deviation from ideal behaviour for large  $V_{GS}$  gives further evidence that charge transport is limited by injection over/through a potential barrier. The calculated effective field-effect mobility ( $\mu$ ) and extracted threshold voltage ( $V_T$ ) are 0.13  $\text{cm}^2 \text{V}^{-1} \text{s}^{-1}$  and 28 V, respectively. These same  $I_D$  versus  $V_{GS}$  characteristics are plotted on a semi-logarithmic scale and show the OTFT to have an on/off current ratio near  $10^6$ . The data in Fig. 2 are typical and not best case. We often observe some hysteresis between the forward and reverse current–voltage sweep as a result of a shift in the threshold voltage of 2–5 V. The magnitude of the shift can, for some devices, be related to the film quality and substrate preparation. The opportunity for improvement by optimization of the dielectric is suggested by the observation that the use of hexylmethylsilazane to chemically modify the silicon dioxide interface can reduce  $V_T$  to near zero and increase the on/off current ratio to greater than  $10^7$  (see Supplementary Information, Fig. S1).

Figure 2c shows  $\mu$  versus  $L$  for two representative batches of diF-TESADT TFTs, one fabricated with PFBT-treated contacts and the other with untreated contacts. The effective field-effect mobility is 3–5 times larger for OTFTs with PFBT-treated contacts and  $L < 25$   $\mu\text{m}$ . Both data sets show a similar qualitative dependence on  $L$ : the mobility increasing with decreasing channel length. This observed trend is the reverse of the decrease in mobility with decreasing  $L$  that is typically reported for high-mobility OTFTs with parasitic contact effects<sup>31</sup>.

Studying the film microstructure on top of the contacts, along the contact edge, and in the channel region provides insight into the cause for the observed dependence of  $\mu$  on contact treatment and  $L$ . Optical micrographs of OTFTs with decreasing  $L$  show the contacts to greatly affect the film microstructure (Fig. 3a,b). Optical inspection of the contact and channel region for a long  $L$  device under crossed polarizers confirms nucleation and growth on top of the contacts that extends into the channel

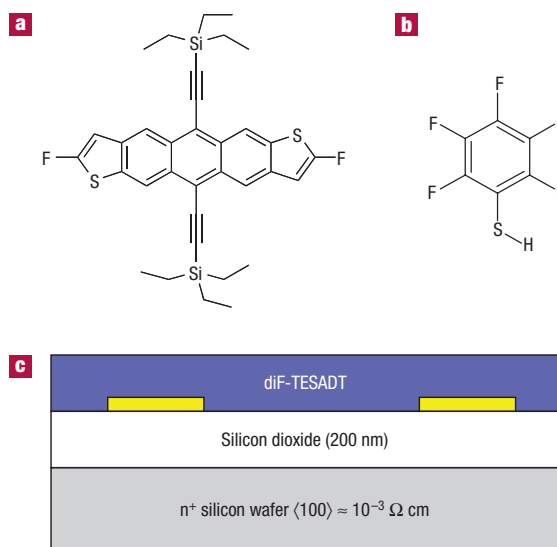


**Figure 1** Chemical structures and OTFT schematic cross-section. **a, b**, Chemical structure for fluorinated diF-TESADT (**a**) and PFBT (**b**). **c**, Schematic diagram of the device cross-section.

and is strongly birefringent (see Supplementary Information, Fig. S2). The oriented regions near the contact edge extend for more than 10  $\mu\text{m}$  into the channel of the device. Devices with longer  $L$  show a transition in film microstructure in the middle of the transistor channel (Fig. 3a). OTFTs with  $L < 20$   $\mu\text{m}$  have channel regions comprised almost entirely of large grains (Fig. 3b). For comparison, Fig. 3c shows the optical micrograph for a diF-TESADT TFT fabricated with untreated contacts ( $L = 20$   $\mu\text{m}$ ). Relatively small grains are found on top of the contacts, and there is comparatively little or no growth/propagation of grains into the transistor channel. Correspondingly, the mobility is lower ( $\mu \approx 2 \times 10^{-2} \text{cm}^2 \text{V}^{-1} \text{s}^{-1}$ ) for short  $L$  devices. The mobility is independent of contact treatment for large  $L$  devices, quantitatively confirming that it is the contact-induced microstructure that gives the superior performance of treated devices at shorter  $L$ .

To quantify the thin-film microstructure, we have used a number of analytical techniques, including X-ray diffraction studies of free-standing diF-TESADT single crystals grown from solution to determine the crystal structure. Results from X-ray diffraction of single crystals show the molecules adopt a packing very similar to unfluorinated TESADT and 6,13-bis(triisopropylsilylethynyl) pentacene: a two-dimensional  $\pi$ -stack<sup>26,27,32</sup>. To study the crystallinity of the thin films in-plane (parallel to the substrate), we use grazing-incidence X-ray diffraction (GIXD). Preliminary results verify that blanket films are comprehensively oriented on PFBT-treated Au with a structure very similar to that of single-crystal diF-TESADT with the  $a$ – $b$  plane parallel to the substrate (see Supplementary Information, Fig. S3). The GIXD patterns of films on untreated silicon dioxide clearly consist of two different orientations of crystals with only a fraction with the  $a$ – $b$  plane parallel to the substrate. We presume the mid-channel region of long  $L$  OTFTs to be similarly ordered.

Polarizing optical techniques (spectroscopic ellipsometry and infrared absorption) have also been applied to the study of films on unpatterned substrates (see Supplementary Information, Fig. S4). In contrast to the diffraction techniques that exquisitely probe only the crystalline regions of the film, the optical techniques characterize the average molecular orientation distribution of the

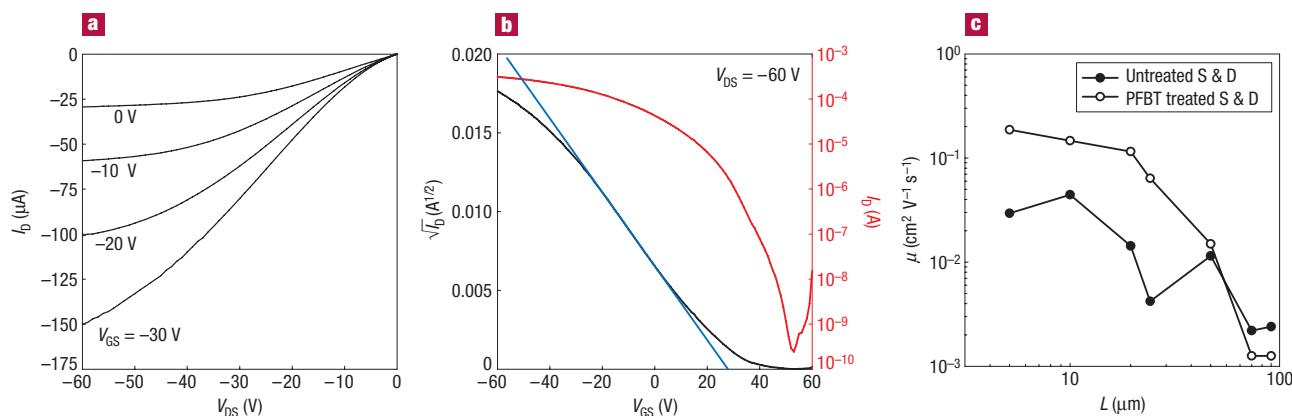


**Figure 2** Representative d.c. electrical characteristics for a diF-TESADT TFT. **a, b**,  $I_D$  versus  $V_{DS}$  characteristics (**a**) and  $I_D$  versus  $V_{GS}$  characteristics (**b**) for a diF-TESADT TFT with PFBT-treated contacts, a 20  $\mu\text{m}$  channel length and a 1,000  $\mu\text{m}$  channel width. **c**, Saturation mobility as a function of channel length ( $L$ ) for diF-TESADT TFTs with a 1,000  $\mu\text{m}$  channel width with PFBT-treated contacts and with untreated contacts. The devices were fabricated using films spun-cast at 1,000 r.p.m. from 2 wt% solutions in room-temperature toluene.

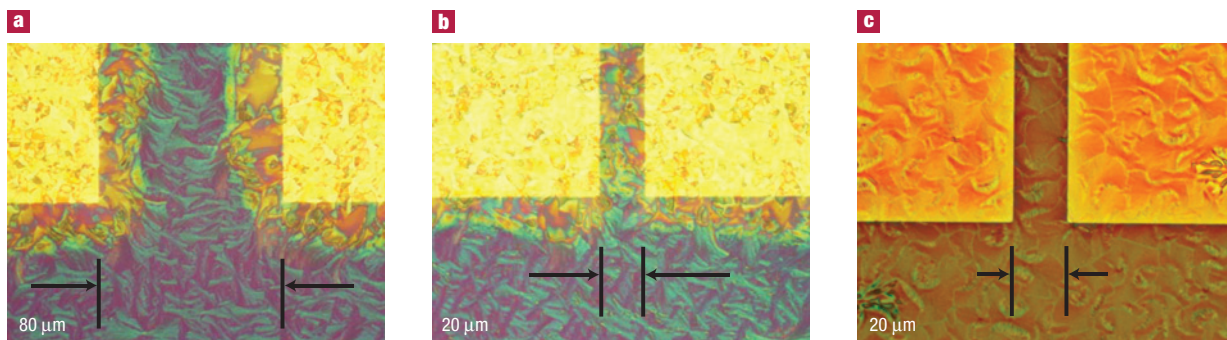


**Figure 3** Optical micrographs of diF-TESADT TFTs. The TFTs have channel lengths of 80  $\mu\text{m}$  (**a**) and 20  $\mu\text{m}$  (**b, c**). **a, b**, Films spin-cast at 1,000 r.p.m. from 2 wt% solutions in warm toluene onto substrates with PFBT-treated source and drain contacts. **c**, Film spin-cast at 1,000 r.p.m. from a 2 wt% solution in room-temperature toluene onto substrates with untreated source and drain contacts. Images were taken using differential interference contrast.

entire film. The molecular orientation is found to vary with film thickness, substrate and chemical treatment. In all cases, there is a net molecular order (that is, the films are not entirely random). The highly crystalline, oriented films on PFBT-treated Au exhibit a molecular order quantitatively consistent with the single-crystal structure with the  $a$ - $b$  plane parallel to the substrate. The long axis of the ADT core is preferentially near the plane of the surface, whereas the side groups preferentially orient near the surface normal. This is the preferred orientation for charge transport via the  $\pi$ -system. The orientation of films on untreated Au and silicon dioxide is significantly different with persistent orientation of the ADT core long axis but a more face-on orientation with the side groups strongly tilted from the surface normal consistent with the GIXD observation of multiple crystal orientations.

The strong tendency of diF-TESADT films to crystallize provides some evidence of interaction between the fluorine atoms and the sulphur atoms in the thiophene rings on adjacent molecules. Weak sulphur-fluorine interactions have been reported in the literature<sup>33</sup>. We suggest that increased sulphur-fluorine interaction in diF-TESADT leads to rapid formation of a ‘tape’ motif that precipitates and seeds the growth of the plate-like crystals, consistent with the short ( $\sim 0.294$  nm to 0.298 nm) F-S

contact observed for the single crystal. This conjecture of increased sulphur-fluorine interaction between diF-TESADT molecules is also substantiated by the increase of melting enthalpy from an average value of  $\Delta H = 23.6$  J g<sup>-1</sup> for TESADT to  $\Delta H = 44$  J g<sup>-1</sup> for diF-TESADT (measured by differential scanning calorimetry).

The PFBT treatment is found to play an essential role in obtaining the microstructure shown in Fig. 3a,b for the improved device performance. This role extends beyond simply ‘tuning’ the surface energy to avoid dewetting from the contacts, as observed for films cast on octadecanethiol-treated Au ( $\theta_{\text{H}_2\text{O}} \approx 105^\circ$  compared with  $\theta_{\text{H}_2\text{O}} \approx 86^\circ$  for PFBT-treated Au). For example, we fabricated and tested devices with benzenethiol-treated Au ( $\theta_{\text{H}_2\text{O}} \approx 61^\circ$ ) and observed only minimal, if any, crystallization along contact edges (similar to the microstructure shown in Fig. 3c). Consequently, TFTs with benzenethiol-treated Au have mobility similar to that shown in Fig. 2c for the devices fabricated with untreated contacts.

The results from the different microstructure studies show diF-TESADT crystals preferentially nucleate on the PFBT-treated Au with the  $a$ - $b$  plane (and thus their fast growth directions) in the plane of the film, enabling the formation of plate-like crystals. Crystals nucleating near contact edges are found to grow 10  $\mu\text{m}$  or more into the channel (see atomic force microscopy

images in Supplementary Information, Fig. S5 and polarized optical micrographs Supplementary Information, Fig. S2). Our general observations and quantitative findings from microstructure studies point to the possibility of some interaction between the sulphur atoms in the thiophene rings of the diF-TESADT and the PFBT-treated Au. It should also be noted here that spun-cast unfluorinated TESADT solutions in toluene on substrates with PFBT-treated contacts show no crystal growth on the contacts or extending from the contact edges. Interestingly, heating the diF-TESADT solution before spin-casting is found to significantly affect crystallization along the contact edge and in the channel region for OTFTs with untreated contacts, while having only a relatively small influence on  $\mu$  ( $\approx 0.2 \text{ cm}^2 \text{ V}^{-1} \text{ s}^{-1}$  for  $L < 20 \mu\text{m}$ ) and film microstructure for OTFTs fabricated with PFBT-treated contacts. The thin-film microstructure, magnitude of  $\mu$  and the dependence of  $\mu$  on  $L$  for untreated contacts with heated solutions are nearly identical to that shown in Figs 2 and 3 for the OTFTs fabricated with PFBT-treated Au. Taken together, this suggests that the contact-controlled microstructure arises from competition between the nucleation rate (set by contact treatment) and growth rate (influenced by solvent temperature).

To gain further insight into the relationship between the contact-induced film microstructure and charge transport, we have studied the temperature dependence of the current–voltage characteristics for devices as a function of  $L$ . Figure 4 shows  $\mu$  for OTFTs with different channel lengths ( $L = 10 \mu\text{m}$ ,  $20 \mu\text{m}$ ,  $50 \mu\text{m}$ ,  $80 \mu\text{m}$ ) measured from 4.2 K to 300 K. The mobility for all OTFTs is thermally activated between 90 K and 300 K, with a characteristic energy ( $E_A$ ) that increases with increasing  $L$  from  $E_A \approx 0.027 \text{ eV}$  for  $L = 10 \mu\text{m}$  to  $E_A \approx 0.080 \text{ eV}$  for  $L = 80 \mu\text{m}$ . We find the large difference in  $E_A$  to be consistent with our picture of decreasing disorder in the channel region with decreasing  $L$ , that is, a reduction in the density of grain boundaries and an increase in the fraction of crystals oriented with the  $a$ – $b$  plane parallel to the substrate. For  $T < 90 \text{ K}$ , the mobility shows a trend towards temperature-independent transport with decreasing  $L$ . Temperature-independent mobility has rarely been observed in TFTs. It was most recently reported for single-grain pentacene TFTs and a decade ago for high-performance polycrystalline pentacene TFTs (refs 34,35).

The ability to favourably control the morphology of spin-coated films processed at room temperature using simple interface treatments is remarkable and suggests a diversity of simple self-patterning possibilities. We demonstrate the use of contact-treatment-controlled microstructure by fabricating high-performance OTFTs and ring-oscillator circuits on a flexible polyimide substrate. Circuit fabrication and characterization is described in detail in the Methods section. Figure 5a,b shows a flexed polyimide substrate with a variety of spin-cast diF-TESADT circuits and an optical micrograph of the seven-stage ring oscillator. The different microstructures on the PFBT-treated electrodes and polyimide field regions can be easily seen. Despite the greater processing complexity required to fabricate circuits on flexible polyimide substrates, we are able to obtain the same contact-controlled microstructure shown in Fig. 3b for OTFTs on oxidized silicon (see Supplementary Information, Fig. S6 showing the optical micrograph of an OTFT pair that make up an inverter stage of the ring oscillator).

Films deposited on PFBT-treated samples from toluene solution on polyimide substrates typically have mobilities of  $0.1$ – $0.2 \text{ cm}^2 \text{ V}^{-1} \text{ s}^{-1}$ , threshold voltages of  $-2$  to  $1 \text{ V}$  and subthreshold slopes of  $1.0 \text{ V}$  per decade to  $2.2 \text{ V}$  per decade. The electrical characteristics obtained on polyimide substrates are as high quality as the devices fabricated on oxidized silicon using the greatly simplified test structure. The near-zero threshold voltage

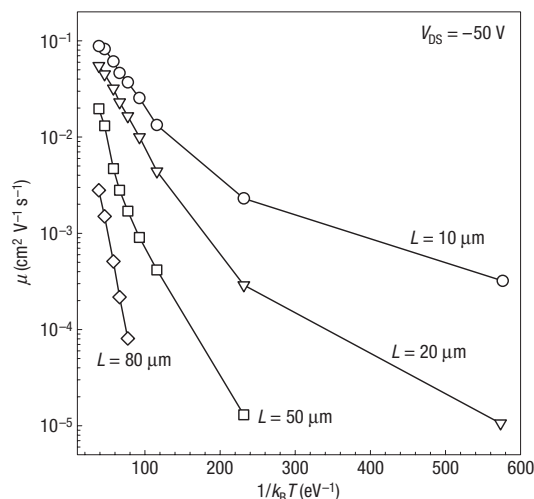


**Figure 4** Temperature dependence of the effective field-effect mobility in the saturation regime. The mobility is plotted as a function of inverse substrate temperature ( $1/k_B T$ ) for devices with PFBT-treated contacts with a  $1,000 \mu\text{m}$  channel width and having channel lengths ( $L$ ) of  $10 \mu\text{m}$ ,  $20 \mu\text{m}$ ,  $50 \mu\text{m}$  and  $80 \mu\text{m}$ . The film was spin-cast at  $1,000 \text{ r.p.m.}$  from a  $2 \text{ wt\%}$  solution in warm toluene.

for the devices on polyimide substrates enables us to fabricate simple digital logic circuits without level shifting, unlike previous reports for TFT circuits fabricated by using thermally evaporated pentacene thin films<sup>13</sup>. Significant to the circuit work are the poor transport properties of the field regions (optically clear regions), which provide natural isolation between adjacent inverters, and eliminates the need for further processing steps to etch the organic semiconductor film. From the current–voltage characteristics of long  $L$  TFTs biased at  $V_{GS} = 0 \text{ V}$ , we estimate the sheet resistance of the low-mobility regions in field to be higher than  $10^9 \text{ ohms per sq.}$  This level of isolation is adequate for many circuit applications and electronic paper, but is not sufficient for high-information-content display applications. Preliminary evidence indicates that a simple hydrophobic treatment of the field region can further improve isolation owing to dewetting of the semiconductor. Figure 5c,d shows output waveforms for the seven-stage ring oscillator operating at two different supply voltages;  $V_{DD} = -5 \text{ V}$  and  $-40 \text{ V}$ , respectively. The dynamic TFT operation demonstrated at  $V_{DD}$  as low as  $-5 \text{ V}$  confirms that our diF-TESADT TFTs can be used in low-voltage electronic applications. Figure 5e shows a plot of the oscillation frequency and the single-stage propagation delay as a function of the supply voltage. The propagation delay (and oscillation frequency) shows the expected decrease (increase) with increasing supply voltage and a single-stage delay of less than  $5 \mu\text{s}$  is achieved for large  $V_{DD}$ . OTFTs fabricated on polyimide substrates with untreated electrodes typically have mobility less than  $10^{-2} \text{ cm}^2 \text{ V}^{-1} \text{ s}^{-1}$ .

The results from our studies of spin-cast diF-TESADT OTFTs show the tremendous potential for engineering self-ordering of soluble organic semiconductor materials. We show that by exploiting the strong tendency of diF-TESADT to crystallize along chemically tailored contact interfaces, we can greatly improve the electrical characteristics of the OTFTs. Channel-length-dependent and temperature-dependent current–voltage characteristics correlate well with the thin-film microstructure. Our ability to dramatically influence the thin-film morphology at microscopic and macroscopic scales enables us to fabricate high-performance

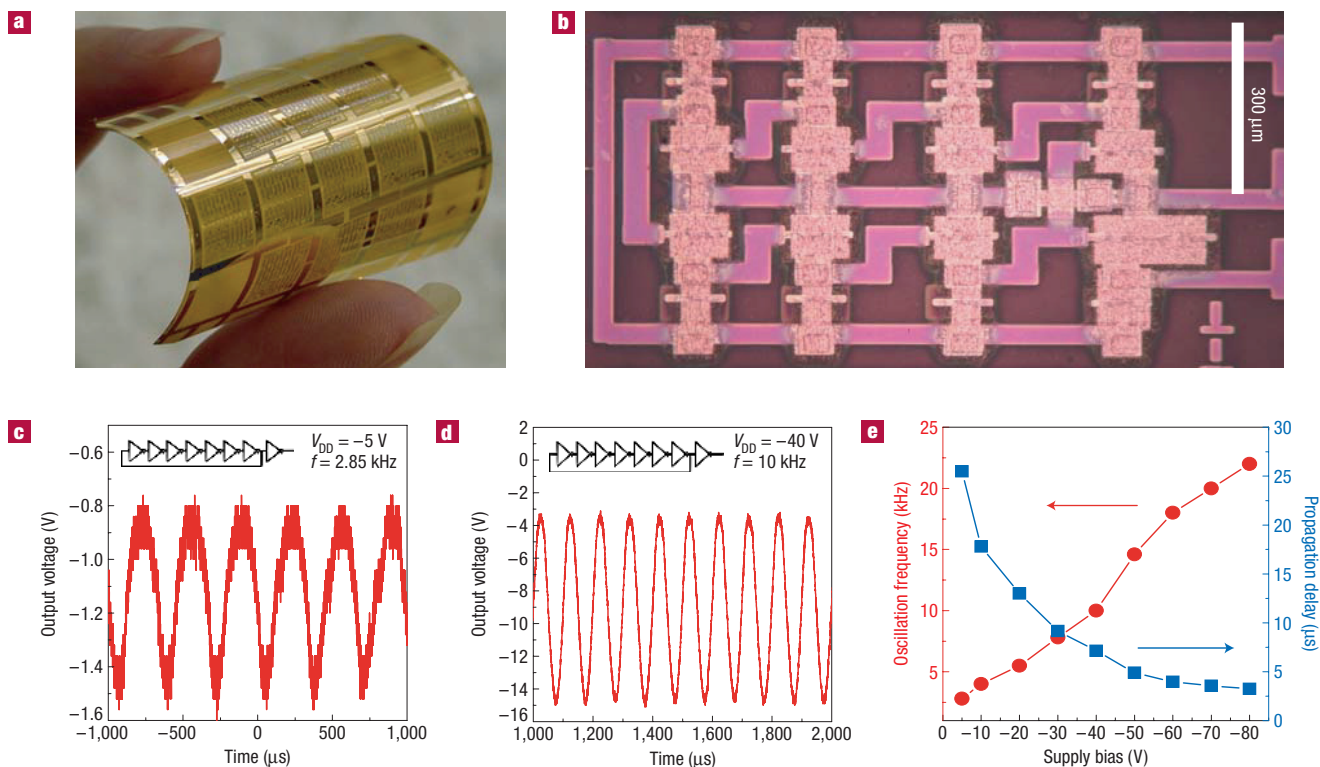


**Figure 5** Photograph, optical micrograph and electrical characteristics for diF-TESADT TFT circuits on a flexible plastic substrate. **a,b**, A polyimide substrate with a variety of spin-cast diF-TESADT circuits (**a**) and an optical micrograph of a seven-stage ring oscillator (**b**). The different microstructures on the PFBT-treated electrodes and polyimide field regions can be easily seen. **c,d**, Output waveforms for the ring oscillator operating from supply voltages of  $-5$  V (**c**) and  $-40$  V (**d**). **e**, Plot of oscillation frequency and per stage propagation delay as a function of supply voltage.

digital circuits on flexible plastic substrates, as well as test structures that are well suited for fundamental studies on charge injection and transport in the OTFT channel. Most importantly, our use of the contacts to induce crystallinity in the channel region of OTFTs opens the field to novel room-temperature, low-cost, self-patterning techniques for manufacturing high-channel-mobility OTFTs and flexible circuits<sup>36</sup>.

## METHODS

### TRANSISTOR AND CIRCUIT FABRICATION, AND ELECTRICAL CHARACTERIZATION

Discrete OTFTs were fabricated on heavily doped and thermally oxidized (100) n-type silicon wafers. The silicon dioxide gate insulator was grown in dry oxygen and had an average thickness of 200 nm. Source and drain contacts were formed by evaporating a 3–5-nm-thick titanium (Ti) adhesion layer followed by a conformal 50-nm-thick gold (Au) layer, and they were patterned by photolithography and a lift-off process. Subsequently, the substrates were cleaned by immersion in solvents and rinsed with deionized water. Trace organic contaminants were removed by ultraviolet–ozone exposure. To modify the source and drain contact interface properties, the substrates were immersed in a  $10^{-2}$  mol l<sup>-1</sup> PFBT solution in room-temperature ethanol for 30–60 min and sonicated in neat ethanol before blow drying with N<sub>2</sub>. Fluorinated diF-TESADT was used as synthesized by SS and JEA. Details of the synthesis and crystal structure will be published elsewhere<sup>37</sup>. All diF-TESADT films were deposited by spin-coating from 17 to 18 mg ml<sup>-1</sup> (2 wt%) solutions in room-temperature or warm (approximately 60 °C) toluene at  $1,000 \times 2\pi$  rad min<sup>-1</sup> or  $2,000 \times 2\pi$  rad min<sup>-1</sup> for 30 s. The ellipsometric film thickness on untreated silicon dioxide was approximately 70 nm. The completed OTFTs were placed in a vacuum oven at 30 °C to remove any residual solvent from the film.

Because of its good dimensional stability, polyimide substrates were used to fabricate flexible diF-TESADT TFTs and ring-oscillator circuits. The integration

of TFTs into electronic circuits on a plastic substrate requires a patterned gate electrode and a gate insulator that can be deposited at temperatures compatible with the substrate. For this work, nickel (Ni) was used for the gate electrode and silicon dioxide deposited by reactive ion-beam sputtering at 80 °C was used as the gate dielectric and insulation layer for wiring cross-overs. Au source and drain electrodes were deposited by thermal evaporation and patterned using lift-off. Before the active-layer deposition, substrates were cleaned using ultraviolet ozone. After ultraviolet cleaning, the interface properties of the Au source/drain electrodes were modified by immersing the substrates in a  $10^{-2}$  mol l<sup>-1</sup> solution of PFBT in ethanol for 15 min. For the active layer, a diF-TESADT film was spun from a 17 to 18 mg ml<sup>-1</sup> solution in room-temperature toluene over the prepatterned circuit electrodes and dried. All solution preparation and device processing steps for circuit fabrication were carried out in an air ambient at room temperature.

The d.c. electrical characteristics of discrete OTFTs on silicon substrates were measured at room temperature in a nitrogen-purged probe station by using a semiconductor parameter analyser. The electrical characteristics of the OTFT circuits on polyimide substrates were measured in room air on a probe station by using a d.c. power supply to provide the circuit bias and an oscilloscope to capture the output waveform. Temperature-dependent d.c. electrical characteristics were measured in a vacuum (base pressure  $< 10^{-7}$  torr) cryogenic probe station (4.2 K to 300 K). For all of the electrical measurements, the gate contact was made to the wafer backside. The effective field-effect mobility in the saturation regime was calculated from the following relationship:

$$\mu = \frac{2}{C_i} \frac{L}{W} \frac{\partial I_D^{1/2}}{\partial V_{GS}} \quad (1)$$

where  $\mu$  is mobility,  $C_i$  is the capacitance per unit area for the silicon dioxide gate dielectric, and  $W$  and  $L$  are the transistor channel width and length, respectively. An aggregate value for  $\partial I_D^{1/2} / \partial V_{GS}$  was determined from the slope of the line fitted to the linear part of a plot of  $\sqrt{I_D}$  versus  $V_{GS}$ .

## FILM MICROSTRUCTURE AND SURFACE TREATMENT ANALYSIS

Differential interference contrast optical microscopy, polarized optical microscopy and atomic force microscopy were used to analyse the thin-film microstructure. The orientation of diF-TESADT molecules comprising films spin-cast on silicon dioxide (assumed to be similar to that in the field region and in the mid-channel of long  $L$  devices) and on untreated and PFBT-treated Au was analysed by using GIXD and polarizing optical techniques: spectroscopic ellipsometry and infrared absorption. Silicon dioxide and Au interfaces that were chemically modified with molecules that self-assemble to form molecular layers were characterized by measuring the contact angle of a deionized water droplet ( $\theta_{\text{H}_2\text{O}}$ ) by using the sessile-drop method.

Received 8 June 2007; accepted 16 January 2008; published 17 February 2008.

## References

- Horowitz, G. Organic field-effect transistors. *Adv. Mater.* **10**, 365–377 (1998).
- Dimitrakopoulos, C. D. & Malenfant, P. R. L. Organic thin film transistors for large area electronics. *Adv. Mater.* **14**, 99–117 (2002).
- Sirringhaus, H. Device physics of solution-processed organic field-effect transistors. *Adv. Mater.* **17**, 2411–2425 (2005).
- Sheraw, C. D. *et al.* Organic thin-film transistor-driven polymer-dispersed liquid crystal displays on flexible polymeric substrates. *Appl. Phys. Lett.* **80**, 1088–1090 (2002).
- Gelinck, G. H. *et al.* Flexible active-matrix displays and shift registers based on solution-processed organic transistors. *Nature Mater.* **3**, 106–110 (2004).
- Baude, P. F. *et al.* Pentacene-based radio-frequency identification circuitry. *Appl. Phys. Lett.* **82**, 3964 (2003).
- Noguchi, Y., Sekitani, T. & Someya, T. Organic-transistor-based flexible pressure sensors using ink-jet-printed electrodes and gate dielectric layers. *Appl. Phys. Lett.* **89**, 253507 (2006).
- McCulloch, I. *et al.* Liquid-crystalline semiconducting polymers with high charge-carrier mobility. *Nature Mater.* **5**, 328–333 (2006).
- Klauk, H., Zschieschang, U., Pflaum, J. & Halik, M. Ultralow-power organic complementary circuits. *Nature* **445**, 745–748 (2007).
- Jackson, T. N. Organic semiconductors: Beyond Moore's law. *Nature Mater.* **4**, 581–582 (2005).
- Gundlach, D. J. Low-power, big impact. *Nature Mater.* **6**, 173–174 (2007).
- Berggren, M., Nilsson, D. & Robinson, N. D. Organic materials for printed electronics. *Nature Mater.* **6**, 3–5 (2007).
- Kane, M. G. *et al.* Analog and digital circuits using organic thin-film transistors on polyester substrates. *IEEE Electron Device Lett.* **21**, 534–536 (2000).
- Stuedel, S., Myny, K., De Vusser, S., Genoe, J. & Heremans, P. Patterning of organic thin film transistors by oxygen plasma etch. *Appl. Phys. Lett.* **89**, 183503 (2006).
- Kymissis, I., Dimitrakopoulos, C. D. & Purushothaman, S. Patterning pentacene organic thin film transistors. *J. Vac. Sci. Technol. B* **20**, 956–959 (2002).
- Loo, Y. L., Willet, R. L., Baldwin, K. W. & Rogers, J. A. Interfacial chemistries for nanoscale transfer printing. *J. Am. Chem. Soc.* **124**, 7654–7655 (2002).
- Hines, D. R. *et al.* Nanotransfer printing of organic and carbon nanotube thin-film transistors on plastic substrates. *Appl. Phys. Lett.* **86**, 163101 (2005).
- Blanchet, G. B., Loo, Y. L., Rogers, J. A., Gao, F. & Fincher, C. R. Large area, high resolution, dry printing of conducting polymers for organic electronics. *Appl. Phys. Lett.* **82**, 463–465 (2003).
- Choi, H. Y., Kim, S. H. & Jang, J. Self-organized organic thin-film transistors on plastic. *Adv. Mater.* **16**, 732–736 (2004).
- Stuedel, S., Janssen, D., Verlaak, S., Genoe, J. & Heremans, P. Patterning growth of pentacene. *Appl. Phys. Lett.* **85**, 5550–5552 (2004).
- Briseno, A. *et al.* Patterning growth of large oriented organic semiconductor single crystals on self-assembled monolayer templates. *J. Am. Chem. Soc.* **127**, 12164–12165 (2005).
- Briseno, A. *et al.* Patterning organic crystal transistor arrays. *Nature* **444**, 913–917 (2006).
- Park, S. K., Kuo, C.-C., Anthony, J. E. & Jackson, T. N. *IEEE International Electron Devices Meeting, 2005, IEDM Technical Digest* 113–116 (The Institute of Electrical and Electronics Engineers, Piscataway, 2005).
- Kuo, C.-C., Payne, M. M., Anthony, J. E. & Jackson, T. N. *IEEE International Electron Devices Meeting, 2004 IEDM Technical Digest* 373–376 (The Institute of Electrical and Electronics Engineers, Piscataway, 2004).
- Payne, M. M., Parkin, S. R., Anthony, J. E., Kuo, C.-C. & Jackson, T. N. Organic field-effect transistors from solution-deposited functionalized acenes with mobilities as high as  $1 \text{ cm}^2 \text{ V}^{-1} \text{ s}^{-1}$ . *J. Am. Chem. Soc.* **127**, 4986–4987 (2005).
- Anthony, J. E., Brooks, J. S., Eaton, D. L. & Parkin, S. R. Functionalized pentacene: Improved electronic properties from control of solid-state order. *J. Am. Chem. Soc.* **123**, 9486–9483 (2001).
- Anthony, J. E., Eaton, D. L. & Parkin, S. R. A road map to stable, soluble, easily crystallized pentacene derivatives. *Org. Lett.* **4**, 15–18 (2002).
- Gundlach, D. J., Jia, L. L. & Jackson, T. N. Pentacene TFT with improved linear region characteristics using chemically modified source and drain electrodes. *IEEE Electron Device Lett.* **22**, 571–573 (2001).
- Kymissis, I., Dimitrakopoulos, C. D. & Purushothaman, S. High-performance bottom electrode organic thin-film transistors. *IEEE Trans. Electron Devices* **48**, 1060–1064 (2001).
- Bock, C. *et al.* Improved morphology and charge carrier injection in pentacene field-effect transistors with thiol-treated electrodes. *J. Appl. Phys.* **100**, 114517 (2006).
- Gundlach, D. J. *et al.* An experimental study of contact effects in organic thin film transistors. *J. Appl. Phys.* **100**, 024509 (2006).
- Dickey, K. C., Anthony, J. E. & Loo, Y.-L. Improving organic thin-film transistor performance through solvent vapor annealing of solution-processable triethylsilyl ethynyl anthradithiophene. *Adv. Mater.* **18**, 1721–1726 (2006).
- Reichenbacher, K., Süß, H. I. & Hulliger, J. Fluorine in crystal engineering—the little atom that could. *Chem. Soc. Rev.* **34**, 22–30 (2005).
- Minari, T., Nemoto, T. & Isoda, S. Temperature and electric-field dependence of the mobility of a single-grain pentacene field-effect transistor. *J. Appl. Phys.* **99**, 034506 (2006).
- Nelson, S. F., Lin, Y.-Y., Gundlach, D. J. & Jackson, T. N. Temperature-independent transport in high-mobility pentacene transistors. *Appl. Phys. Lett.* **72**, 1854–1856 (1998).
- Park, S. K. *et al.* *65th Device Research Conference Digest* 23–24 (The Institute of Electrical and Electronics Engineers, Piscataway, 2007).
- Subramanian, S. *et al.* Chromophore fluorination enhances crystallization and stability of soluble anthradithiophene semiconductors. *J. Am. Chem. Soc.* (in the press).

## Acknowledgements

Financial support under the Summer Undergraduate Research Fellowship (SURF) by the National Science Foundation is gratefully acknowledged by J.E.R. L.C.T., A.J.M. and B.H.H. acknowledge financial support from the National Research Council postdoctoral fellowship program. J.E.A. acknowledges the Office of Naval Research for financial support of synthesis efforts. D.J.G. acknowledges L. Loo, Princeton U., for many helpful discussions concerning nucleation and film microstructure, and B. Vogel, visiting assistant professor at Bucknell University, for assistance with preliminary differential scanning calorimetry measurements. Correspondence and requests for materials should be addressed to D.J.G. Supplementary Information accompanies this paper on [www.nature.com/naturematerials](http://www.nature.com/naturematerials).

Reprints and permission information is available online at <http://npg.nature.com/reprintsandpermissions/>